Ceramics-Silikáty 64 (1), 18-28 (2020)
www.ceramics-silikaty.cz doi: 10.13168/cs.2019.0044

THE EFFECT OF Fe^{3+} ION SUBSTITUTION ON THE CRYSTAL STRUCTURE OF YE'ELIMITE

JAURES SYNTYCHE NDZILA*, SHUXIN LIU*, GUOJIAN JING*, #SHUXIAN WANG*, #ZHENGMAO YE*,**

*School of Materials Science and Engineering, University of Jinan, Jinan, Shandong 250022, China
**Shandong Provincial Key Laboratory of Preparation and Measurement of Building Materials, Jinan, Shandong 250022, China

#E-mail: mse_wangsx@ujn.edu.cn, mse_yezm@ujn.edu.cn

Submitted June 5, 2019; accepted September 16, 2019

Keywords: Ye'elimite, Fe^{3+} ions substitution, Crystal structure transformation, X-ray diffraction analysis, Rietveld refinement, Phase transition

Ye'elimite ($Ca_4Al_6SO_{16}$) is one of the major components of calcium sulfoaluminate cements with a rapid hydration, high early strength, and corrosion resistance. In this study, the mechanism of the phase transition between two phases (Pcc2 and I$\underline{4}$3m) was examined by controlling the substitution rate of the Fe^{3+} ions. The results indicated that $Ca_4Al_6SO_{16}$ was the main product of all the samples at 1250 °C in a range from 0 to 25 at. %, which was accompanied by minor calcium aluminate (CA and $C_{12}A_7$) phases. The substitution of the Fe^{3+} ions into $Ca_4Al_6SO_{16}$ promoted the transformation of the crystal structure from Pcc2 to I$\underline{4}$3m. With the substitution rate reaching 10 at. %, the transformation from Pcc2 to I$\underline{4}$3m was effective, according to space group of I$\underline{4}$3m with a = b = c = 9.2147(1) Å and V = 782.4313(3) Å3 (Z = 2). This effective transformation was formed without a structural change in the temperature dependent XRD analysis. The morphology change in the SEM and the structural disorder in the IR confirmed that there was a change among the different samples doped with the Fe^{3+} ions. Substitution of the Fe^{3+} ions for the Al^{3+} ions revealed that the early hydration kinetics were faster for the Fe^{3+}-doped ye'elimite phase compared to the pure ye'elimite phase, which was explained by the presence of minor amounts of the $C_{12}A_7$ phase in the Fe^{3+}-doped ye'elimite phase.

INTRODUCTION

Ye'elimite ($Ca_4Al_6O_{12}SO_4$, $C_4A_3\overline{S}$) is a mineral with rapid hydration, high early strength, rapid setting and very good hardening [1-2]. It has been known as hydraulic phase for several decades and its potential in non-expansive cementitious materials has recently been reported [3]. Currently, several research studies have been devoted to the ye'elimite structure because it is the major component in calcium sulfoaluminate (CSA) cements having a lower environmental impact [4-6] and the second relevant phase (~ 25 wt. %) in sulfobelite (BCSA) cements [7-9]. Ye'elimite belongs to the tectoaluminosilicate sodalite family with the general composition of $M_4(T_6O_{12})X$ where M = Ca, T = Al, and X = SO_4 [10]. In previous studies, it has been shown that ye'elimite has a lower symmetry than those of the previously reported tetragonal system, which can be described as the acentric orthorhombic space group of *Pcc2*. This symmetry shows a √2a * √2a * a superstructure based on the cubic structure at room temperature and the lattice parameters values are a = = 13.0356(7) Å, b = 13.0350(7) Å, and c = 9.1677(2) Å, and the cell volume is V = 1557.78(6) $Å^3$ [10].

As reported previously, the ye'elimite structure was firstly analysed by Hanstead et al. using X-ray powder diffraction [11]. This structure at high-temperature (1073 K) has been subsequently determined by Kurokawa et al. [12] as a cubic with a space group of *I$\underline{4}$3m* and the unit-cell dimensions were a = 9.2426(20) Å and V = 789.55(2) $Å^3$ (Z = 2). This structure has been determined at room temperature by Calos et al. [13] and established like an orthorhombic crystal structure, a space group of *Pcc2* (Z = 4), which has been revised by A. Cuesta et al., using Rietveld refinement and atomistic calculations [10]. In other words, the cubic symmetry can be restored with substitutions of Ca^{2+} by Na^+ and Al^{3+} by B^{3+} or Si^{4+} to expand the frame structure to a non-collapsed state [14]. In addition, some research has indicated that ye'elimite includes a number of ions such as Ti^{4+}, Cr^{3+}, Mn^{3+}, Fe^{3+}, and Si^{4+} in its structure [3]. Two structures (orthorhombic and cubic) of ye'elimite obtained by using the CrystalMaker 2.2 software are shown in Figure 1. And the phase transition in the two structures is qualified to be reversible (from *Pcc2* to *I$\underline{4}$3m*) occurring at ~ 470 ± 10 °C with a relatively small hysteresis [10, 12, 15]. Moreover, both phases (*Pcc2* and *I$\underline{4}$3m*) of ye'elimite at room temperature have low and high energy states by the density functional theory (DFT) calculations [10]. The high-temperature cubic phase is an unstable phase at room temperature and there is need to control it at room temperature.

In a recent work [16], a mixture of cubic and orthorhombic ye'elimite was found in cement clinkers. By increasing the Fe^{3+} ion content, the cubic polymorph increases at the expense of the orthorhombic. In the case of the Fe^{3+} ions, it has been shown that its maximum substitution degree depends on the crystal structure of ye'elimite [11]. This could be explained by the competition between the Al^{3+} and Fe^{3+} ions. With the substitution of the Al^{3+} ions by 10 at. % of the Fe^{3+} ions in the ye'elimite structure, the partial diffraction peaks of the orthorhombic phase were gradually weakened [17]. In prior studies, it has also been shown that the maximum Fe^{3+} ions solid solution in ye'elimite was reached at 12 at. % [18]. In our case, the maximum Fe^{3+} ions substitution in the ye'elimite phase could be reached at 10 at. %. Recently, two modifications of ye'elimite were used. D. Jansen and his group [19] demonstrated that both modifications of ye'elimite (orthorhombic and cubic) react differently with water and the kinetics of the hydration are significantly different due to the modifications. The hydration products were similar. It was also shown that the hydration sequences and main products were similar in the pure and doped ye'elimite phases, and the kinetics for the Fe^{3+}-doped ye'elimite phase were faster due to the presence of small amounts of mayenite ($Ca_{12}Al_{14}O_{33}$ ($C_{12}A_7$)) in this phase [20].

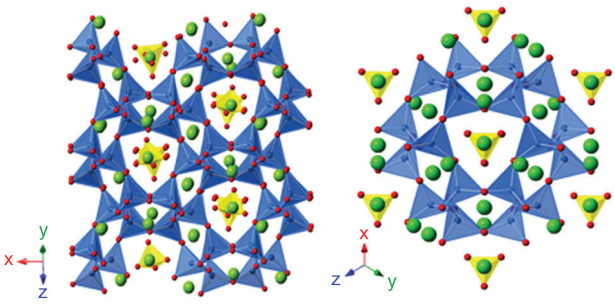

Figure 1. The crystal structures of the ye'elimite phases: a) orthorhombic *Pcc*2, b) cubic *I*$\bar{4}$3*m* (Within the prisms, the green spheres represent the calcium atoms, the blue tetrahedra ones represent the AlO_4 polyhedra, the yellow tetrahedra ones represent the SO_4 polyhedra, and the red spheres represent the oxygen atoms).

There are important discoveries and limitations revealed by the studies of the substitution of the Fe^{3+} ions in ye'elimite [15, 21]. However, the available data and the results are often incoherent and contradictory. Research studies on the formation of $Ca_4Fe_6O_{12}SO_4$ ($C_4F_3\bar{S}$) phase are contradictory [22-23]. Recently, it has also been shown that the effect of the Fe^{3+}-doped on the kinetics of the reaction is conflicting [3, 18]. In this work, the mechanism of the phase transition between the two phases (from *Pcc*2 to *I*$\bar{4}$3*m*) and the accurately controlled ratio of the phases have been examined. The substantial effect of the Fe^{3+} ions on the orthorhombic to cubic transformation was investigated in detail by using a number of experimental techniques such as X-ray diffraction analysis, Rietveld refinement, scanning electron microscopy, and heat flow calorimetry. The objective of this work is to investigate the conditions of the structural change and clarify the analysis of the different phases into the crystal structure of ye'elimite. The results of this study are important in the utilisation of ye'elimite-contained materials and to elucidate the conditions of the effect of the Fe^{3+} ions on the mechanism of the orthorhombic to cubic transformation from a structural point of view.

EXPERIMENTAL

Samples preparation

The samples of ye'elimite corresponding to the formula $Ca_4(Al_{1-x}Fe_x)_6SO_{16}$ (with x = 0.00, 0.02, 0.05, 0.07, 0.1, 0.12, 0.15, and 0.25) were synthesised from stoichiometric amounts of analytical reagent grade $CaCO_3$, $Al(OH)_3$, $CaSO_4{\cdot}2H_2O$, and Fe_2O_3 (the purity of all the reagents was above 99.99 %). Different amounts of the reagents were used to obtain approximately 5 g ye'elimite, and the raw materials were homogenised for 2 hours with ethanol as a dispersive and homogeneity medium. After the evaporation of the ethanol, the mixtures were ground with a mortar and placed in a furnace in an alumina crucible at 1000 °C. Then the samples were ground again in order to make the mixtures further homogeneous. The resulting samples were heated at 1250 °C for 5 hours (a heating rate of 5 °C·min^{-1},

Table 1. The proportions (wt. %) of the raw materials in the S00-S25 samples.

Sample	Chemical formula	$CaCO_3$	$Al(OH)_3$	$CaSO_4{\cdot}2H_2O$	Fe_2O_3
S00	$Ca_4Al_6SO_{16}$	31.93	49.79	18.31	–
S02	$Ca_4Al_{5.8}Fe_{0.1}SO_{16}$	31.60	48.27	18.12	2.02
S05	$Ca_4Al_{5.7}Fe_{0.3}SO_{16}$	31.12	46.08	17.84	4.96
S07	$Ca_4Al_{5.5}Fe_{0.4}SO_{16}$	30.80	44.65	17.66	6.88
S10	$Ca_4Al_{5.4}Fe_{0.6}SO_{16}$	30.34	42.57	17.40	9.68
S12	$Ca_4Al_{5.2}Fe_{0.7}SO_{16}$	30.05	41.22	17.25	11.51
S15	$Ca_4Al_{5.1}Fe_{0.9}SO_{16}$	29.61	39.23	16.98	14.17
S25	$Ca_4Al_{4.5}Fe_{1.5}SO_{16}$	28.25	33.02	16.20	22.53

3 °C·min^{-1}, 2 °C·min^{-1} in the range of 50 - 800 °C, 800 - 1000 °C, 1000 - 1250 °C, respectively) before being slowly cooled. The obtained final samples were named from S00 to S25. The corresponding proportions (wt.%) of the raw materials in the samples are presented in Table 1. When x was increased, the amount of the Fe^{3+} ions in the mixtures became higher and the grinding of the samples produced became difficult. The analysis and the interpretation of the results were carried out essentially on the samples located for $0 \leq x \leq 0.1$.

Methods of investigation

Particle size distribution

The particle size distribution of the samples was obtained by using a Beckman Coulter LS 13 320 particle size analyser. Prior to this measurement, the samples (approximately 100 mg) were each mixed in 40 ml of ethanol and the suspension was sonicated for 3 minutes in order to break the coarse agglomerates.

X-ray diffraction

The samples were analysed by X-ray diffraction with a Bruker-D8 Advance diffractometer equipped with a graphite crystal monochromator, using strictly monochromatic CuK_α radiation (λ = 1.54059 Å) and a Vantec-1 detector. The specimens were collected from 5° to 80° (2θ) with a step size of 0.02°. Additionally, the Rietveld refinement and phase quantification were conducted to analyse the obtained XRD patterns with the Topas-4.2 software. The refined parameters included the background coefficients, the peak shape parameters, the Lp factor, the zero-shift error, the stain, the sample absorption, the unit cell parameters and the atomic sites [24]

Temperature-dependent XRD analysis

The temperature-dependent XRD analysis of the samples was performed on a Panalytical X'pert PRO diffractometer equipped with an X'celerator array detector in an Anton Paar HTK16 high temperature chamber under static air. The specimens were heated at the temperatures of 25 °C, 50 °C, 150 °C, 250 °C, 350 °C, 450 °C, 550 °C, and 650 °C in a platinum sample table with a heating rate of 10 °C·min^{-1}. The thermally treated samples at these temperatures were then recorded by XRD on an angular range from 15° to 35° with a step size of 0.013° and scanning rate of 2 °·min^{-1}.

Scanning electron microscopy

The morphology of the samples was studied by scanning electron microscopy (FEI QUANTA FEG 250) equipped with an Oxford energy dispersive spectrometer (EDS) using secondary electrons. The powder samples were dispersed in alcohol and dropped on a silicon wafer with a pipette.

Infrared spectroscopy

An infrared spectroscopy Nicolet 380 was used for the sample analysis. 1 mg of each sample was ground with 100 mg KBr into an agate mortar to achieve homogenisation. The mixture was then pressed into a transparent disc with a pressure of 10 MPa. The infrared spectrums were collected in the range of 420 - 1400 cm^{-1}.

Heat flow calorimetry

The heat flow calorimetry study with a water/sample (w/s) ratio of 1 was performed in an eight-channel Thermal Activity Monitor (TAM) instrument using glass ampoules. The paste samples were prepared in-situ by mixing ~1 g of each sample with the appropriated water and were immediately introduced into the calorimeter. The heat flow was collected for up to 30 hours at 25 °C.

RESULTS AND DISCUSSION

Particle size distribution

The particle size distribution and the average particle sizes measured by laser diffraction (from 0.04 µm to 2000 µm) of the samples are presented in Table 2 and Figure 2. The specific surface area values were 3.93 m^2·g^{-1}, 1.65 m^2·g^{-1}, 2.31 m^2·g^{-1}, and 2.18 m^2·g^{-1} for S00, S05, S07, and S10, respectively. The values of the particle size distribution were almost similar for all the samples except for d90. This result confirmed the results found on the heat flow calorimetry measurement below, which showed that the shape of the specific surface area of the pure ye'elimite phase was greater than that of the Fe^{3+}-doped ye'elimite phase.

Table 2. The sample sizes.

	S00 (µm)	S05(µm)	S07 (µm)	S10 (µm)
d10	0.61	1.33	1.08	1.25
d50	6.45	8.24	8.87	8.21
d90	13.67	25.90	37.48	29.47

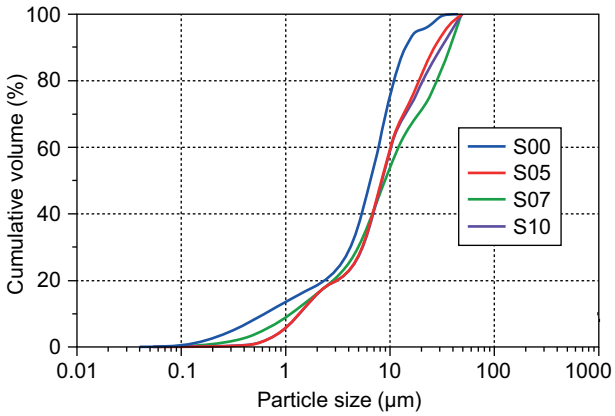

Figure 2. The particle size distribution (PSD) of the samples determined by laser diffraction (LD).

Table 3. The Rietveld quantitative phase analysis results (wt. %) of the samples S00-S25.

wt. %	o-$Ca_4Al_6SO_{16}$	c-$Ca_4Al_6SO_{16}$	CA	$C1_2A_7$	C_2F	R_{wp}	R_p	χ^2
S00	95.85	–	2.80	1.35	–	13.92	10.50	1.89
S02	65.74	29.11	3.29	1.44	1.71	12.81	9.67	1.86
S05	46.70	46.86	3.59	1.54	4.32	12.63	9.39	1.81
S07	28.46	64.88	4.31	3.25	4.43	12.63	9.25	1.83
S10	–	82.51	4.75	4.54	5.62	14.76	10.65	2.17
S12	–	85.10	4.92	4.74	6.12	13.70	10.09	2.02
S15	–	86.61	5.20	5.04	8.43	13.45	9.72	2.01
S25	–	88.55	6.26	5.81	11.47	11.70	8.69	1.76

X-ray diffraction

The Fe^{3+}-doped ye'elimite phase, $Ca_4(Al_{1-x}Fe_x)_6SO_{16}$, was synthesised following the methodology reported for stoichiometric ye'elimite [10]. The temperature was reduced to 50 °C which was relative to the synthesis temperature for the stoichiometric ye'elimite due to the crucible corrosion in the reaction medium [25]. The X-ray diffraction patterns and the Rietveld quantitative phase analysis results for all the samples heated at 1250 °C are given in Figure 3a and Table 3. The results show the formation of the $Ca_4Al_6SO_{16}$ phase as the main product of all the samples in a range from 0 to 25 at. %, which is accompanied by the formation of small amounts of calcium aluminates ($Ca_2Al_2O_4$ (CA) and $Ca_{12}Al_{14}O_{33}$ ($C_{12}A_7$)) as the secondary phases [18]. When increasing the substitution to 5 at. %, the diffraction peaks of $Ca_2Fe_2O_5$ (C_2F) began to appear, and the diffraction intensities increased gradually with the increase in the substitution rate. The C_2F phase appeared as a solid solution constitution of some reduction of Fe^{3+} to Fe^{2+} in this interval [17-18]. The pure ye'elimite phase is orthorhombic *Pcc*2 (o-$Ca_4Al_6SO_{16}$, JCPDS No. 85-2210). When the substitution of the Fe^{3+} ions increased up to 10 at. %, the Fe^{3+}-doped ye'elimite phase was aligned to the cubic *I4̄3m* (c-$Ca_4Al_6SO_{16}$, JCPDS No. 71-0969), and the diffraction intensities of the CA and $C_{12}A_7$ peaks remained stable at 1250 °C in this interval. This showed that increasing the substitution of the Fe^{3+} ions accelerated the formation of the ye'elimite phase at the expense of the CA and $C_{12}A_7$ phases at 1250 °C. From 0 to 7 at. %, the o-$Ca_4Al_6SO_{16}$ and c-$Ca_4Al_6SO_{16}$ phases coexisted in the obtained products. Beyond 10 at. % there were many impurities in the samples besides the cubic phase as shown in Fi-gure S1. The state at this time has reached the limit of the $Ca_4Al_6SO_{16}$ solid solution Fe^{3+} ions. In addition, when the doping concentration reached 10 at. %, the cubic phase had been obtained and the cubic phase still exists at higher contents, see Table 3. The substitution of the Fe^{3+} ions into ye'elimite promoted the stabilisation of the high-temperature cubic of ye'elimite at room temperature, which illustrated the effect of the Fe^{3+} ion substitution on the crystal structure of ye'elimite [17, 26-28].

Moreover, in the Fe^{3+}-doped ye'elimite phase, the tetrahedral Al^{3+} ions are replaced by the Fe^{3+} ions and

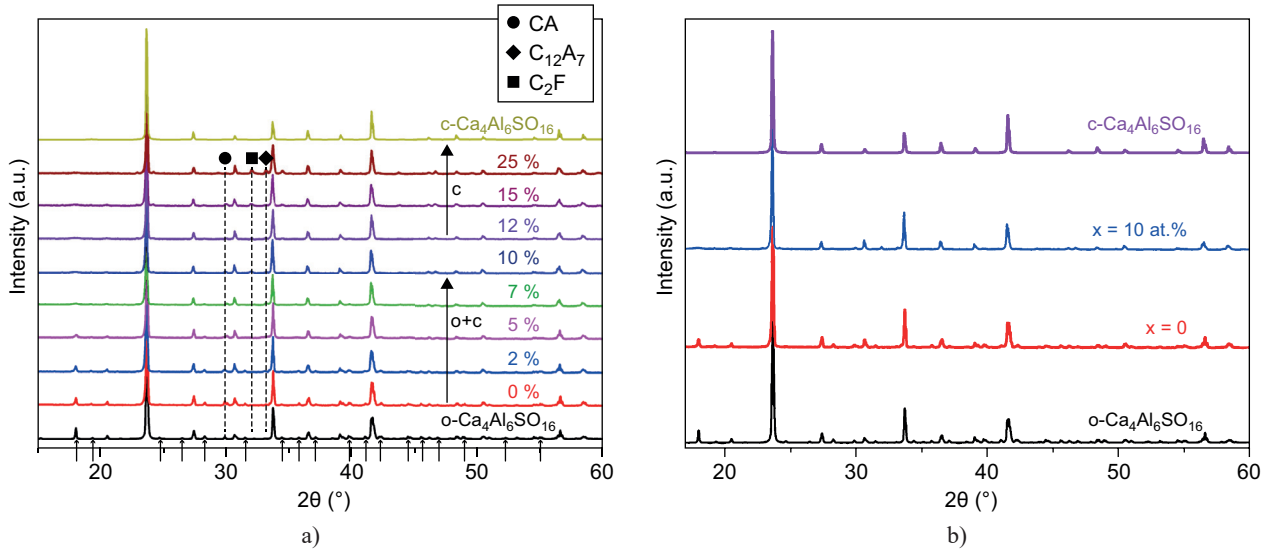

Figure 3. The XRD patterns of the pure and doped ye'elimite heated at 1250 °C. Samples: S00-S25 (a). The partial XRD patterns of the $Ca_4Al_6SO_{16}$ and $Ca_4(Al_{0.9}Fe_{0.1})_6SO_{16}$ powders (b).

the substitution of the Fe^{3+} ions gradually increased. This phenomenon is similar to that observed by Liu et al. with the Ga^{3+} ions [29]. With the increasing amounts of Fe^{3+} ions, some changes were observed in the XRD patterns. Thus, the diffraction intensities of the minor peaks (marked by arrows) observed with the samples at the low substitution rates of the Fe^{3+} ions like 0.00 and 0.02 were gradually attenuated and almost disappeared when the Fe^{3+} ion contents exceeded 10 at. % (S10) as shown in Figure 3b, indicating that these phases were consumed during the formation of the ye'elimite phase by increasing the Fe^{3+} ion contents in the samples. Similarly, it was observed that the minor diffraction peaks were gradually weakened by increasing the temperature [10]. From these results, this was attributed to the crucible corrosion in the reaction medium and the presence of $Al(OH)_3$ and Fe_2O_3 [25-26, 30].

Temperature-dependent XRD analysis

The phase transition of ye'elimite was investigated by the temperature-dependent XRD analysis with the specimens measured from 25 to 550 °C [29]. Here, the temperature-dependent XRD patterns of the $Ca_4(Al_{1-x}Fe_x)_6SO_{16}$ sample (X = 0, 5 at. %, and 10 at. %) was collected in a range from 25 to 650 °C, and the results are shown in Figure 4a-c. As shown in Figure 4a,b, it was observed that the phase transition process from *Pcc*2 to *I*$\bar{4}$3*m* of o-$Ca_4Al_6SO_{16}$ and $Ca_4(Al_{0.95}Fe_{0.05})_6SO_{16}$ took place at 450~550 °C and 350~450 °C, respectively. The crystal system of the Sr-bearing ye'elimite transformed from an orthorhombic system to a cubic system with an increasing degree of the substitutions [31]. The substitution of the Fe^{3+} ions in the ye'elimite structure reduced the phase transition temperature [32] and the $Ca_4(Al_{0.9}Fe_{0.1})_6SO_{16}$ sample showed no phase transformation from 25 to 550 °C see Figure 4c. Finally, the cubic unstable phase could be stabilised at room temperature when the substitution of the Fe^{3+} ions reached 10 at. %, which was similar to the Ga^{3+}-doped ye'elimite powders [29].

As a function of temperature, the lattice parameters and the cell volumes of both polymorphs (orthorhombic *Pcc*2 and cubic *I*$\bar{4}$3*m*) of the $Ca_4(Al_{1-x}Fe_x)_6SO_{16}$ sample (x = 0, 5 at. %, and 10 at. %) have been obtained from the Rieteveld refinement of the temperature-dependent XRD patterns and the results are presented in Figure 5a-c and Table S(1-3). To facilitate the comparison with the cubic average values, the results for the orthorhombic polymorph have been plotted as a/√2, b/√2, and V/2 [10]. The lattice parameters and the cell volumes of both polymorphs showed a certain degree of expansion due to the phase transition of a lower-symmetry phase to a higher-symmetry phase in the interval from room temperature to 650 °C (Figure 5a-b). At 5 at. %, both polymorphs of ye'elimite (orthorhombic and cubic) coexisted when the temperature was between room temperature to 450 °C. When the temperature was above 470 °C, the orthorhombic polymorph cannot be generated. At 10 at. %, the lattice parameter (a') and the cell volume (V') of the high-symmetry phase also showed an expansion with the temperature ranging

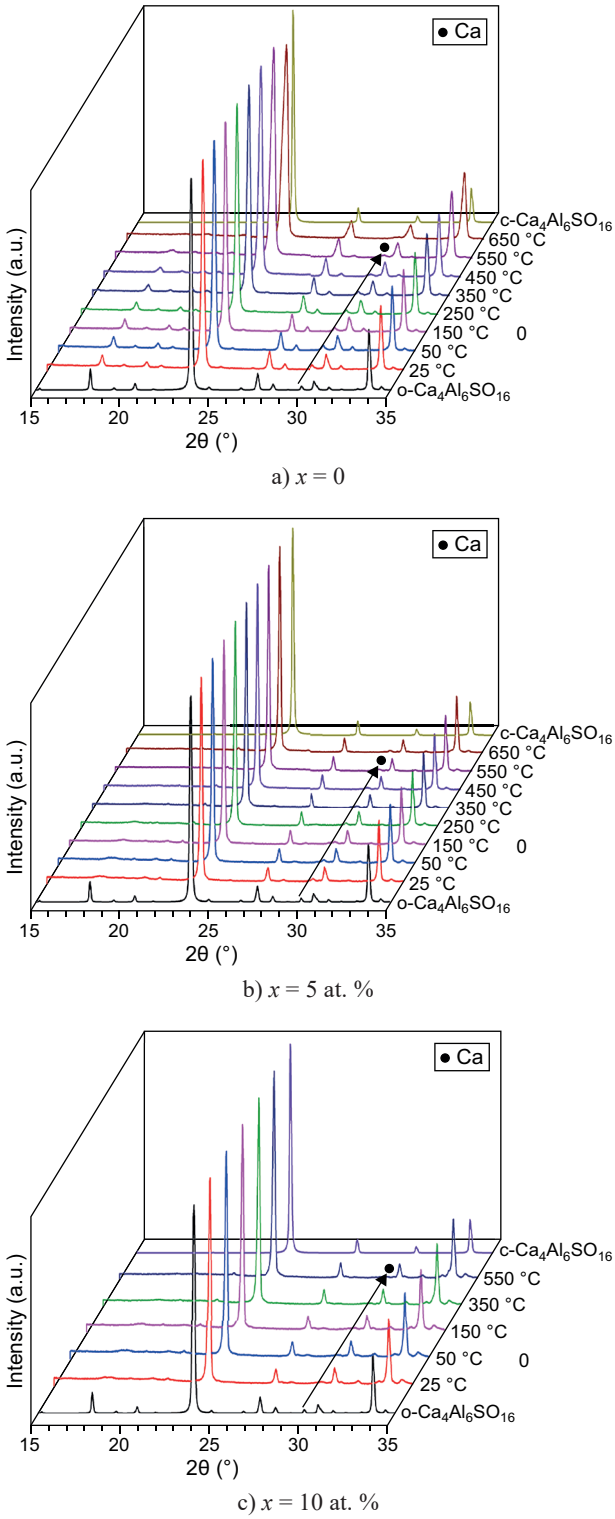

a) x = 0

b) x = 5 at. %

c) x = 10 at. %

Figure 4. The temperature-dependent XRD patterns of $Ca_4(Al_{1-x}Fe_x)_6SO_{16}$ with: a) x = 0, b) x = 5 at. %, and c) x = = 10 at. %.

from 0 to 550 °C and, finally, the $Ca_4(Al_{0.9}Fe_{0.1})_6SO_{16}$ sample shows no phase transformation in this interval (Figure 5c). This was in accordance with the obtained results for the stoichiometric ye'elimite [10].

The phase identification and crystal structures of ye'elimite at room temperature were obtained by the XRD Rietveld refinements by using the Topas-4.2 software. The Rietveld plots for o-$Ca_4Al_6SO_{16}$ and c-$Ca_4Al_6SO_{16}$ are presented in Figure 6a, b using the *Pcc*2 cif file (ICSD 80361) and $Ca_3SrAl_6SO_{16}$ (*I*4̲3*m*, ICSD 81654), respectively as the standard model and the cubic reference model instead of the pure $Ca_4Al_6SO_{16}$ (*I*4̲3*m*, ICSD 9560) phase [12, 33]. It was observed that for the c-$Ca_4Al_6SO_{16}$ phase, the lattice parameters became wider and could lead to an increase of the inter planar spacing with the substitution of the Fe^{3+} ions in the $Ca_4Al_6SO_{16}$ phase. The quantitative analyses and refinement residuals of the samples are given in Figure 6c and Table S4. With the substitution of the Fe^{3+} ions in $Ca_4Al_6SO_{16}$, the degree of the structural disorder was reduced and the corresponding structural symmetry was improved in the solid-solution phase. That is to say that the Fe^{3+}-doped concentration directly affects the

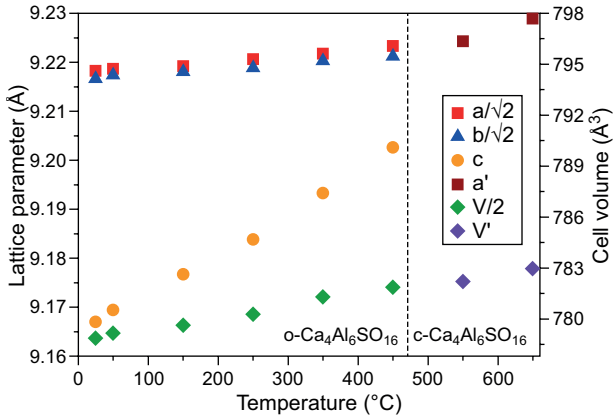

a) $x = 0$

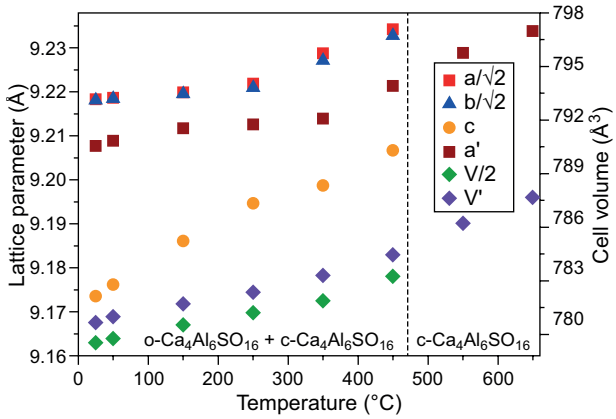

b) $x = 5$ at. %

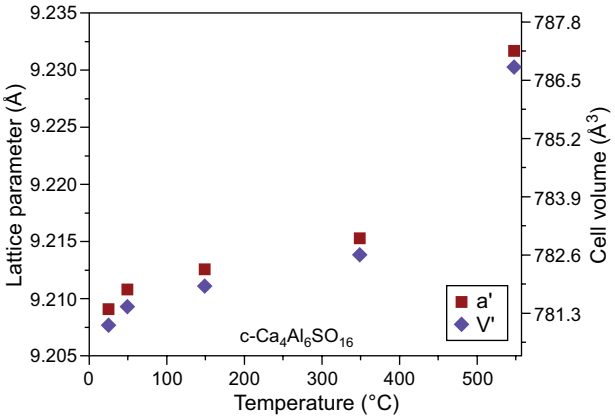

c) $x = 10$ at. %

Figure 5. The refined lattice parameters and the cell volumes for the orthorhombic (from RT to 450 °C) and cubic (470 to 650 °C) $Ca_4(Al_{1-x}Fe_x)_6SO_{16}$ phases with: a) $x = 0$, b) $x = 5$ at. %, and c) $x = 10$ at. % as a function of temperature.

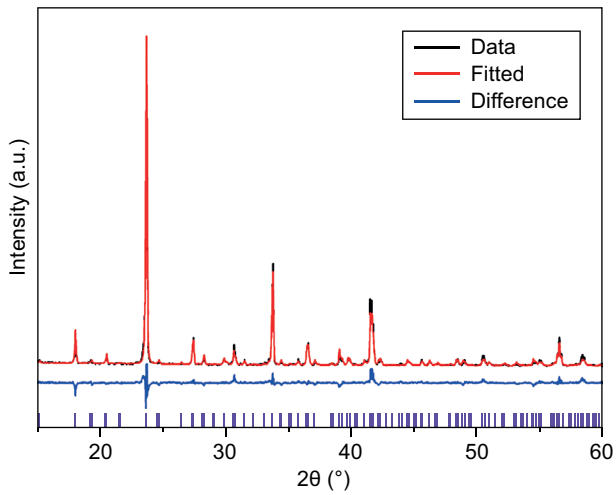

a) $x = 0$

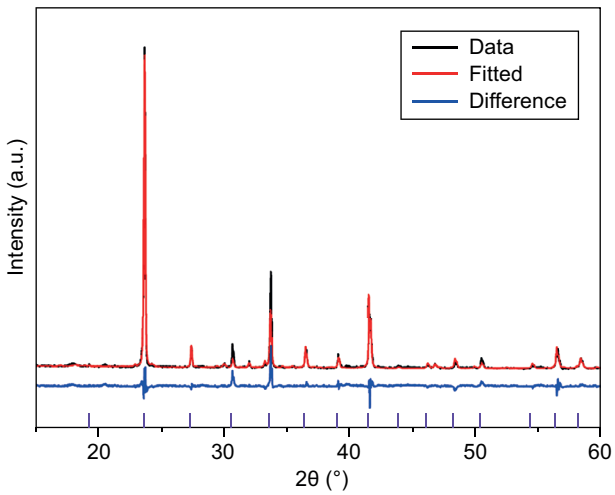

b) $x = 10$ at. %

Figure 6. The Rietveld refinement plots for: a) $x = 0$, and b) $x = 10$ at. %. (RT) The violet and magenta lines represent the diffraction crystal planes of o-$Ca_4Al_6SO_{16}$ and c-$Ca_4Al_6SO_{16}$. *(Continue on next page)*

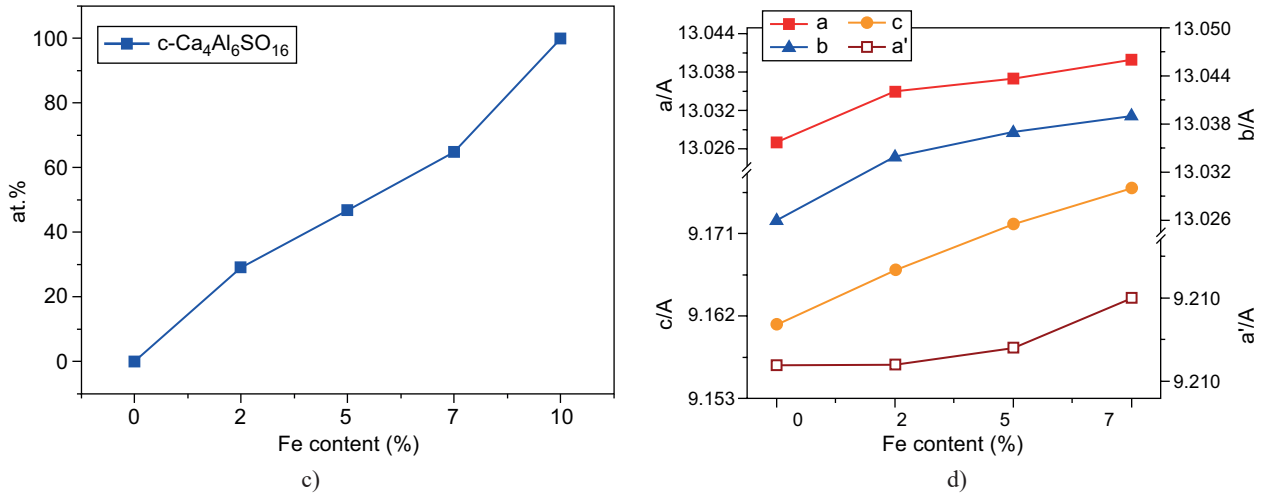

Figure 6. The quantitative analyses result of c-$Ca_4Al_6SO_{16}$ (c). The lattice parameter of o-$Ca_4Al_6SO_{16}$ and c-$Ca_4Al_6SO_{16}$ (d).

proportion of both the polymorphs of ye'elimite. Hence, the transformation of o-$Ca_4Al_6SO_{16}$ to c-$Ca_4Al_6SO_{16}$ is always formed by the substitution of the Fe^{3+} ions. After analysis by the Rietveld refinements, the values of the c-$Ca_4Al_6SO_{16}$ content in $Ca_4(Al_{1-x}Fe_x)_6SO_{16}$ for the x values of 2 at. %, 5 at. %, and 7 at. % were respectively 29.11(8) %, 46.86(0) %, and 64.88(3) %. As regards to Figure 6d and Table S5, the lattice parameters and the cell volumes of both the polymorphs (orthorhombic and cubic) of ye'elimite presented a linear variation with the increasing substitution rate of the Fe^{3+} ions ranging from 0 to 10 at. % which is in good consistency with the previously obtained results [29, 31]. The linear variation in the lattice parameters was explained by the increased inter planar spacing when the Fe^{3+} ions were successfully inserted into the $Ca_4Al_6SO_{16}$ crystal lattice.

Scanning electron microscopy

Figure 7 shows the morphology and the phase composition of the synthesised samples. The morphology and mineral composition analysis showed a clear distinction between the two phases in the micrographs. The pure ye'elimite phase S00 (o-$Ca_4Al_6SO_{16}$) showed that the grain boundaries of the sample were not clear with a particle size of ~1 μm. Secondly, the S05-S10

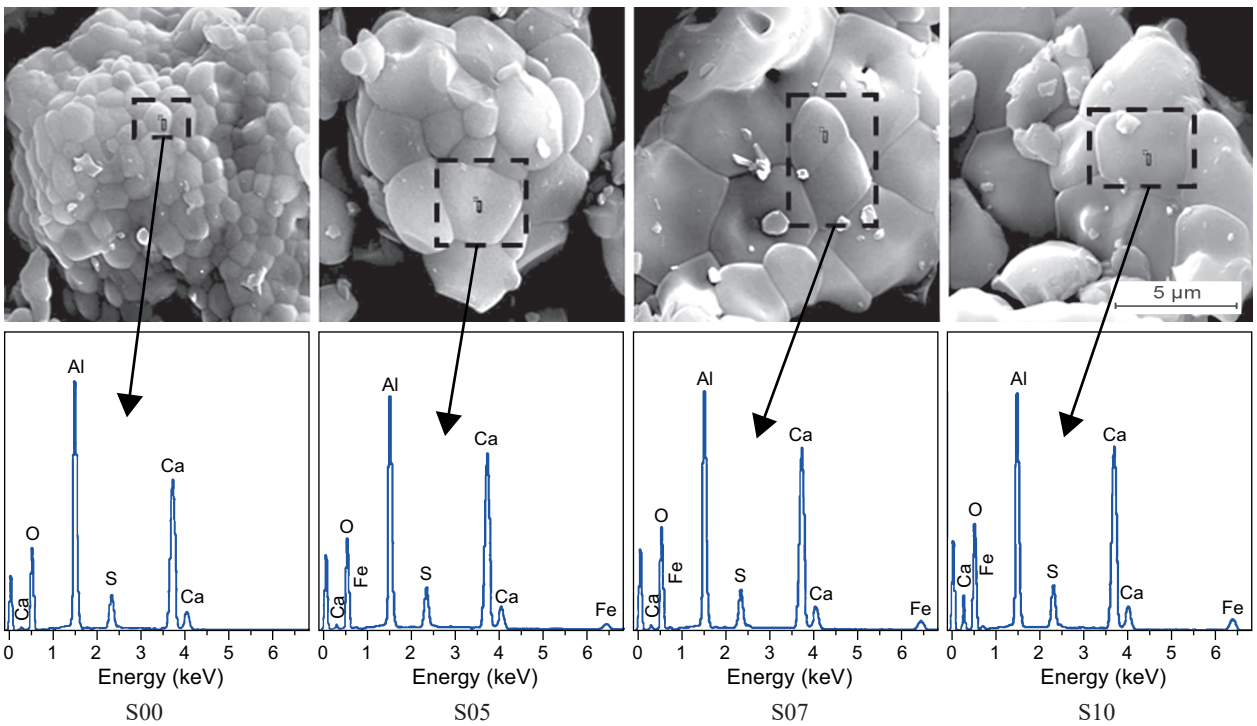

Figure 7. The SEM-EDS morphology and composition analysis of the S00, S05, S07, and S10 samples.

samples (c-$Ca_4Al_6SO_{16}$) corresponding to the Fe^{3+}-doped ye'elimite phase showed a large proportion of particles with a particle size of ~5 μm and were clear. It was clearly evident that the substitution of the Fe^{3+} ions in the ye'elimite phase promoted the formation of minor amounts of calcium aluminate phases and facilitated the relative particle growth in the samples, which was similar with the previously obtained results [17]. The EDS morphology images and the real chemical composition allowed the confirmation of the composition analysis, but also helped to calculate the molar ratio in the samples. The values obtained of the Al/Ca and (Al + Fe)/Ca ratios of the S00, S05, S07, and S10 samples were 1.414, 1.666, 1.706, and 1.698 respectively, which were similar to the stoichiometric ye'elimite (Al/Ca = = 1.5).

Table 4. The real chemical composition of the samples.

Sample	Ca	Al	O	S	Fe
S00	23.93	23.11	48.80	4.16	–
S05	25.04	20.08	48.20	4.37	2.30
S07	24.08	19.45	49.18	3.95	3.35
S10	23.74	18.65	49.34	4.23	4.04

As shown in Figure 7, the substitution of the Fe^{3+} ions had no effect on the uniformity of the samples in the sintering process according to the elemental distribution. Therefore, the substitution of the Fe^{3+} ions played an important role in the stabilisation of ye'elimite by facilitating the phase transition process from orthorhombic to cubic ye'elimite, which was consistent with the above-mentioned results of the XRD analysis.

Infrared spectroscopy

Figure 8 shows the vibration frequencies of the different groups of the S00, S05, S07, and S10 samples in the range of 420 - 1200 cm^{-1}. The vibration bonds of the [AlO_4] groups were located at 617, 642, 690, 821, 883 cm^{-1} and those related to the [SO_4] groups were located at 993, 1101, 1189, 1213 cm^{-1} [34]. It was clearly observed that the vibrations of [AlO_4] were concentrated and shifted at 800 - 890 cm^{-1}. These vibrations were weakened when the substitution of the Fe^{3+} ions increased in the samples. The absorption positions resulting in the [SO_4] groups were observed at 950 - 1250 cm^{-1} and no shift with an increasing substitution rate of the Fe^{3+} irons. With the substitution of the Fe^{3+} ions in ye'elimite, a structural disorder was observed and the absorption bonds of the [AlO_4] groups expanded as compared with the [SO_4] groups. This illustrated the changes in the coordination of the environment.

Therefore, the vibration frequency of the chemical bonds was related to the force constant K by the following formula:

$$\bar{v} = \frac{1}{\lambda} = \frac{1}{2\pi c}\sqrt{k/\mu} = 1307\sqrt{k/\mu} \quad (1)$$

where k is determined by the bond length and bond energy, and μ is the convert mass ($\mu = m_1m_2/(m_{1+}m_2)$, related to the mass of the bonding atoms) [35].

The relative values for the bond energies of Fe–O and Al–O, which determined the measurement of the bond strength in the chemical bond were 406 $kJ{\cdot}mol^{-1}$ and 511 $kJ{\cdot}mol^{-1}$, respectively. After the calculation, it was observed that $\mu_{Fe-O} > \mu_{Al-O}$ and $K_{Fe-O} < K_{Al-O}$. The results showed a slight displacement of the vibration wavenumbers towards the low frequency zone, which was in agreement with results obtained from [29, 31].

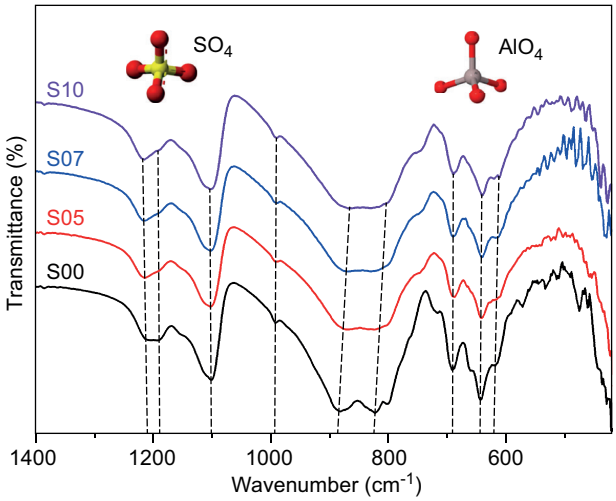

Figure 8. The infrared spectra of the S00, S05, S07, and S10 samples.

Heat flow calorimetry

Figures 9 and 10 show the results of the heat flow calorimetry at the water:sample ratio of 1:1. The heat flow curves are shown on Figure 9 with two maximums during the hydration process. The first maximum was observed when the water was added with the $Ca_4Al_6SO_{16}$ powder and the heat was evolved. The reaction occurred for a short time and was characterised by a very low heat flow at an earlier period followed by an induction period for about 5 hours. This phenomenon was also observed by Jansen et al. [19] with the two modifications of ye'elimite. The induction period was followed by a strong increase in the heat flow, reaching its second maximum at about 10 hours of hydration, and finally decreased normally without showing any other maximum up to the level of the induction period. This is consistent with the above reports [36]. At the end of the induction period up to approximately 16 hours of the hydration heat flow, the maximum was observed with the pure ye'elimite phase with a slight shoulder clearly seen at 13 hours. Indeed, in the first observed peaks, the peaks of the Fe^{3+}-doped

ye'elimite phase had the greatest intensity than those of the pure ye'elimite phase, which showed faster hydration kinetics. This was explained by the presence of minor amounts of the calcium aluminate ($C_{12}A_7$) phase in the Fe^{3+}-doped ye'elimite phase, which accelerated the early hydration kinetics at the early times [20]. In contrast, the heat flow curves corresponding to substitution rates of the Fe^{3+} ions like 0 and 7 at. % appeared higher than that of the ye'elimite phase at 10 at. %. Its reaction speed becomes weak. This was explained by the fact that the ye'elimite phase at 10 at. % was more stable and compact when the water was added. This conformed with the results obtained by M. Idrissi et al. [3] on the Fe^{3+}-doped calcium sulfoaluminate at 21 °C, which indicated that the substitution of the Fe^{3+} ions into the ye'elimite phase could improve its hydraulic reactivity, formed and stabilised the cubic phase of ye'elimite [27].

Figure 10 shows the evolution of the total heat depending on the increase in the Fe^{3+} ion content in the samples. After 30 hours of hydration, the values of the cumulative heat of the Fe^{3+}-doped ye'elimite phase were almost the same (503.1 $J \cdot g^{-1}$ for S07 and 504.3 $J \cdot g^{-1}$ for S10) compared to 556.5 $J \cdot g^{-1}$ (S00) for the pure ye'elimite phase. At the time of commencement, the reaction was extraordinarily slow. After 7 hours, a strong acceleration of the reaction was observed for S07 and S10 up to about 16 hours, but for S00, the reaction continued to be extraordinarily slow up to about 13 hours and increased to reach its maximum at 22 hours. Finally, the reaction continued to progress slowly and produced heat up to 30 hours.

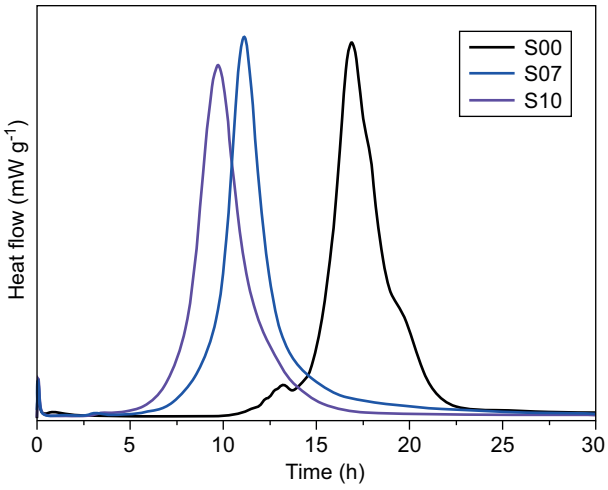

Figure 9. The heat flow curves of the pure and for the pure and the doped ye'elimite phase.

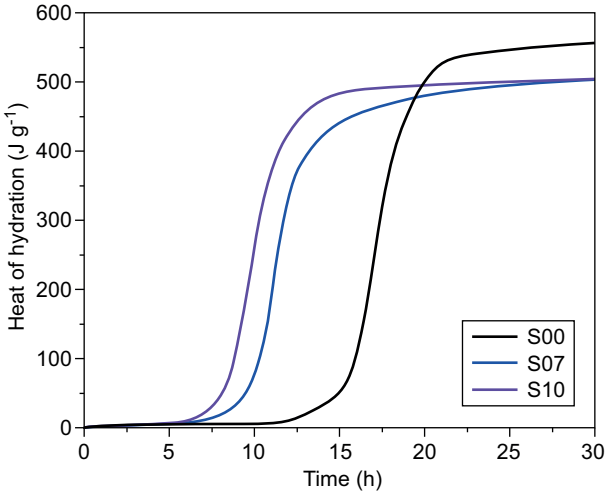

Figure 10. The heat of the hydration doped ye'elimite phase.

CONCLUSIONS

The results found in this work have allowed for the clarification of the conditions of the effect of the Fe^{3+} ion substitution on the crystal structure of ye'elimite. It can be seen that the substitution of the Fe^{3+} ions into ye'elimite not only improved the stability of the cubic phase at room-temperature, it also facilitated the transformation process from orthorhombic to cubic by increasing the Fe^{3+} ion content in the samples. It emerged that when the substitution rate of the Fe^{3+} ions reached 10 at. % ($Ca_4(Al_{0.9}Fe_{0.1})_6SO_{16}$), the transformation of o-$Ca_4Al_6SO_{16}$ to c-$Ca_4Al_6SO_{16}$ was effective. This was according to the space group of $I\bar{4}3m$ with a = b = c = = 9.2147(1) Å and V = 782.4313(3) $Å^3$ (Z = 2). This effective transformation was confirmed by no structural changes in the temperature-dependent XRD analysis. The results of the SEM-EDS morphology and the infrared measurements confirmed a change in the different samples doped with Fe^{3+} ions. The substitution of the Fe^{3+} ions into ye'elimite phase revealed that the early hydration kinetics were faster for the Fe^{3+}-doped ye'elimite phase compared to the pure ye'elimite phase, which influenced the hydraulic reactivity, formed and stabilised the cubic phase of ye'elimite. After 30 hours of hydration, the values of the cumulative heat of the Fe^{3+}-doped ye'elimite phase were almost the same (503.7 ± 0.6 $J \cdot g^{-1}$) as compared to 556.5 $J \cdot g^{-1}$ (S00) for the pure ye'elimite phase. Finally, a key strategy to understand the phase-change mechanism was to combine the comprehensive analysis method with the structural research by controlling the substitution rate of the raw materials of ye'elimite at the optimal conditions. To this end, we noticed that the phase transition of $Ca_4Al_6SO_{16}$ from *Pcc*2 to $I\bar{4}3m$ was reversible.

Acknowledgements

This research work was financially supported by National Natural Science Foundation of China (Grant No.51772129) and the National Key Research and Development Programme (No.2016YFB0303505).

REFERENCES

1. Janotka I., Krajèi L.E. (2000): Resistance to freezing and thawing of mortar specimens made from sulphoaluminate-belite cement. Bulletin of Materials Science, 23(6), 521-527. doi: 10.1007/BF02903894
2. Álvarez-Ayuso E., Querol X., Tomás A. (2006): Environmental impact of a coal combustion-desulphurisation plant: Abatement capacity of desulphurisation process and environmental characterisation of combustion by-products. Chemosphere, 65(11), 2009-2017. doi: 10.1016/j.chemosphere.2006.06.070
3. Idrissi M., Diouri A., Talbi M.A., Sassi O., Taibi M., Damidot D. (2012). Hydration behavior of iron doped cal-cium sulfoaluminate phase at room temperature. In: 2nd International Seminar Innovation & Valorization in Civil Engineering & Construction Materials, Volume 2, pp. 1-368.
4. García-Mate M., Santacruz I., De la Torre A.G., Léon-Reina L., Aranda M.A.G. (2012): Rheological and hydration characterization of calcium sulfoaluminate cement pastes. Cement and Concrete Composites, 34(5), 684−691. doi: 10.1016/j.cemconcomp.2012.01.008
5. García-Mate M., De la Torre A.G., Leon-reina L., Aranda M.A.G., Santacruz I. (2013): Hydration studies of calcium sulfoaluminate cements blended with fly ash. Cement and Concrete Research, 54, 12−20. doi: 10.1016/j.cemconres.2013.07.010
6. Odler I. (2000). Cements containing calcium sulfoaluminate. In: Special Inorganic Cements, 3rd ed, FN Spon, London, pp. 69-87.
7. Alvarez-Pinazo G., Santacruz I., Leon-Reina L., Aranda M.A.G., De la Torre A.G. (2013): Hydration reactions and mechanical strength developments of iron-rich sulfobelite eco-cements. Industrial & Engineering Chemistry Research, 52 (47), 16606−16614. doi: 10.1021/ie402484e
8. Morin V., Walenta G., Gartner E., Termkhajornkit P., Baco I., Casabonne J.M. (2011). Proceedings of the 13th international Congress on the Chemistry of Cement, Madrid, Spain.
9. Cuberos A.J.M., De la Torre A.G., Álvarez-Pinazo G., Martín-Sedeño M.C., Schollbach K. H. Pöllmann, M.A.G. Aranda. (2010): Active iron-rich belite sulfoaluminate cements: clinkering and hydration. Environmental Science & Technology, 44 (17), 6855−6862. doi: 10.1021/es101785n
10. Cuesta A., De la Torre A.G., Losilla E.R., Peterson V.K., Rejmak P., Ayuela A., Frontera C., Aranda M.A.G. (2013): Structure, Atomistic Simulations and Phase Transition of Stoichiometric Ye'elimite. Chemistry of Materials, 25, 1680−1687. doi: 10.1021/cm400129z
11. Halstead P.E., Moore A.E. (1962): The composition and crystallography of an anhydrous calcium aluminosulphate occurring in expanding cement. Journal of Applied Chemistry, 12 (9), 413−417. doi: 10.1002/jctb.5010120906
12. Kurokawa D., Takeda S., Colas M., Asaka T., Thomas P., Fukuda K. (2014): Phase transformation of $Ca_4[Al_6O_{12}]SO_4$ and its disordered crystal structure at 1073 K. Journal of Solid State Chemistry, 215, 265-270. doi: 10.1016/j.jssc.2014.03.040
13. Calos N.J., Kennard C.H.L., Whittaker A.K., Davis R.L. (1995): Structure of calcium aluminate sulfate $Ca_4Al_6O_{16}S$. Journal of Solid State Chemistry, 119, 1−7. doi: 10.1016/0022-4596(95)80002-7
14. Hargis C.W., Moon J., Lothenbach B., Winnefeld F., Wenk H.R., Monteiro P.J.M. (2014): Calcium sulfoaluminate sodalite ($Ca_4Al_6O_{12}SO_4$) crystal structure evaluation and bulk modulus determination. Journal of American Ceramic Society, 97, 892-898. doi: 10.1111/jace.12700
15. Wang Y.G., YE H.Q., Kuo K.H., Feng X.J., Lao G.L., Long S.Z. (1990): Electron diffraction and HREM studies of the new phase and superstructures in $Ca_4Al_6SO_{16}$. Journal of Materials Science, 25, 5147−5156. doi: 10.1007/BF00580143
16. Bullerjahn F., Schmitt D., Haha M.B. (2014): Effect of raw mix design and of clinkering process on the formation and mineralogical composition of (ternesite) belite calcium sulphoaluminate ferrite clinker. Cement and Concrete Research, 59, 87-95. doi: 10.1016/j.cemconres.2014.02.004
17. Idrissi M., Diouri A., Damidot D., Greneche J.M., Talbi M.A., Talbi M. (2010): Characterisation of iron inclusion during the formation of calcium sulfoaluminate phase. Cement and Concrete Research, 40, 314−1319. doi: 10.1016/j.cemconres.2010.02.009
18. Chen D., Feng X., Long S. (1993): The influence of ferric oxide on the properties of $3CaO*3Al_2O_3*CaSO_4$. Thermochimica Acta, 215, 157−169. doi: 10.1016/0040-6031(93)80088-R
19. Jansen D., Spies A., Neubauer J., Ectors D., Goetz-Neunhoeffer F. (2017): Studies on the early hydration of two modifications of ye'elimite with gypsum. Cement and Concrete Research, 91, 106-116. doi: 10.1016/j.cemconres.2016.11.009
20. Bullerjahn F., Zajac M., Haha M.B., Scrivener K.L. (2019) Factors influencing the hydration kinetics of ye'elimite: effect of mayenite. Cement and Concrete Research, 116, 113-119. doi: 10.1016/j.cemconres.2018.10.026
21. Álvarez-Pinazo G., Cuesta A., García-Mate M., Santacruz I., Losilla E.R., De la Torre A.G., León-Reina L., Aranda M.A.G. (2012): Rietveld quantitative phase analysis of ye'elimite-containing cements. Cement and Concrete Research, 42, 960–971. doi: 10.1016/j.cemconres.2012.03.018
22. Makhmudova V., Iskandarova M., Ivanova Y., Chernev G., Ruziev N. (2011): Synthesis and properties of sulphoferrite calcium clinkers and low temperature cements on their basis. Journal of the University of Chemical Technology and Metallurgy, 46 (2), 151–154.
23. De la Torre A.G., Cuberos A.J.M.,Álvarez-Pinazo G., Cuesta A., Aranda M.A.G. (2011): In situ powder diffraction study of belite sulfoaluminate clinkering. Journal of Synchrotron Radiation, 18, 506–514. doi: 10.1107/S0909049511005796
24. Thompson P., Cox D.E., Hastings J.B. (1987): Rietveld refinement of Debye-Scherrer synchrotron X-ray data from Al_2O_3. Journal of Applied Crystallography, 20, 79-83. doi: 10.1107/S0021889887087090
25. Cuesta A., De la Torre A.G., Losilla E.R., Santacruz I., Aranda M.A.G. (2014): Pseudocubic Crystal Structure and Phase Transition in Doped Ye'elimite. Crystal Growth & Design, 14, 5158-5163. doi: 10.1021/cg501290q
26. Li Y., Liu X., Niu X., Song L. (2007): Influence of minor oxides on formation and decomposition of mineral calcium sulfoaluminate ($3CaO·3Al_2O_3·CaSO_4$). Materials Research Innovation, 11 (2), 92–94. doi: 10.1179/143307507X196644
27. Bullerjahn F., Haha M.B., Scrivener K.L. (2015): Iron solid solutions of ye'elimite – Effect on reactivity. In: 14th International Congress on the Chemistry of Cement, Beijing, China.

28. Khessaimi Y.E., Hafiane Y.E., Smith A., Trauchessec R., Diliberto C., Lecomte A. (2018): Solid-state synthesis of pure ye'elimite. Journal of European Ceramic Society, 38 (9), 3401-3411. doi: 10.1016/j.jeurceramsoc.2018.03.018
29. Liu S., Lu X., Chen J., Wang S., Ye Z., Cheng X. (2018): Modulation of Two Yeelimite Phase via Ga^{3+} Cation Substitution. Crystal Engineering Community, 20, 1-11. doi: 10.1039/C8CE00405F
30. Yeping H., Xiaodong S., Suhua M., Lin C., Baiqian Z. (2007): Effect of Fe_2O_3 on the formation of calcium sulfoaluminate mineral. Journal of Chinese Ceramic Society, 35, 1-4.
31. Zhao J., Chang J. (2017): Crystallographic Analysis of Sr-Bearing Ye'elimite. Journal of Inorganic and Organometallic Polymers, 27 (6), 1694-1702. doi: 10.1007/s10904-017-0631-8
32. Banno H., Ichikawa S., Takeda S., Asaka T., Colas M., Thomas P and Fukuda K. (2017): Crystal structures and polymorphism of $Sr_4[Al_6O_{12}]SO_4$. Journal of the Ceramic Society of Japan, 125 (4), 364-370. doi: 10.2109/jcersj2.17008
33. Young R.A. (1993). The Rietveld Method. Oxford University Press: Young, R.A., Ed., Oxford, U.K.
34. Liu X.L., Zhang Y. N. (2002): Influence of MgO on the formation of Ca_3SiO_5 and $3CaO{\cdot}3Al_2O_3{\cdot}CaSO_4$ minerals in alite-sulphoaluminate cement. Cement and Concrete Research, 32 (7), 1125-1129. doi:10.1016/S0008-8846(02)00751-2
35. Werheit H., Filipov V., Kuhlmann U., Schwarz U., Armbrüster M., Leithe-Jasper A., Tanaka T., et al. (2010): Raman effect in icosahedral boron-rich solids. Science and Technology of Advanced Materials, 11 (2), 1-27.
36. Winnefeld F., Barlag S. (2010): Calorimetric and thermogravimetric study on the influence of calcium sulfate on the hydration of ye'elimite, Journal of Thermal Analysis and Calorimetry, 101, 949-957.